

A statistical evaluation of the EPIC flux calibration

XMM-SOC-CAL-TN-0023

Version 2.0

R. D. Saxton

April 4 2003

Abstract

The 1XMM catalogue of XMM-Newton sources provides an important dataset for investigating the performance of the EPIC instrumentation. We have used the catalogue to perform a detailed comparison of the recorded flux in each camera and have investigated the fidelity of the instrumental calibration. The two MOS cameras agree remarkably well implying that the on-axis cross-calibration of these cameras is good to within 4%. The dispersion of the on-axis flux distribution is tight and consistent with residual small calibration uncertainties. Off-axis the distribution is broader illustrating the importance of a correct modelling of the chip-to-chip variation in the MOS point spread function. The EPIC-pn camera agrees with the MOS cameras at low energies but records 5-10% less flux above 2 keV. This may be partly explained by the simplified encircled energy correction used in the catalogue construction but implies the presence of a residual calibration error, possibly related to the MOS quantum efficiency or the throughput of the gratings. The dispersion of the on-axis MOS/PN flux distribution is wider than expected and not understood. Off-axis the discrepancy between the MOS and EPIC-pn fluxes increases although the dispersion is similar.

1 Introduction

The objective of this paper is to assess the relative calibration of the EPIC instrumentation by using a large sample of sources jointly observed by the MOS and PN cameras. This second version of the document is based on sources from the XMM catalogue [1] which has been constructed using the pipeline processing system (PPS), SAS version `xmmsas_20020507_1701`, run at the Science Survey Centre (SSC; [2]). The catalogue contains the position and parameters of about 30,000 sources and represents a rich resource for the XMM-Newton project. It samples a wide range of observational parameters and may be used for investigating instrumental effects such as detector quantum efficiency, the point spread function, the vignetting function and telescope astrometry as well as having a fundamental astronomical value.

Where sources have been detected in more than one camera, their observed fluxes have been compared to identify any systematic differences in the camera calibrations.

2 Sample selection

The large number of sources available in the catalogue has allowed tighter constraints to be used when selecting sources compared to the previous version of this study. The relative flux difference between the EPIC cameras has been calculated from the following source subset:

- All catalogue sources have been manually screened to identify spurious detections, sources contaminated by extended emission and sources lying near to the edge of the field-of-view or to a CCD boundary. Sources meeting any of these conditions have been excluded from the sample.
- Sources at an off-axis angle greater than 5 arcminutes in the MOS cameras have been excluded
- Sources with < 250 counts in the MOS-1 observation have been excluded (see below)
- The catalogue is constructed from FullFrame, ExtendedFullFrame and LargeWindow EPIC-pn observations. EPIC-pn SmallWindow observations are hence implicitly excluded from this comparison. All the major MOS imaging modes are included in the catalogue.
- The majority of the catalogued sources have been observed prior to revolution 300.

2.1 Source counts

The creation of a sample from catalogued sources means that at the low flux end the data will contain sources which have been artificially boosted by a statistical fluctuation - the Eddington effect. Simulations have been run to quantify this effect on low significance sources in the catalogue and the relationship between recovered and input counts is shown in Figure 1. There is a constant offset between the ratio of recovered to input counts due to a known problem with the PSF used in the simulations (I.M.Stewart, p.comm.) but it can be seen that the ratio tends to this offset for an input of about 250 counts. *Fluxes calculated from a smaller number of counts than this will be biased upwards.* This effect will result in a broadening of the flux comparison between the MOS detectors for low-count sources but will cause an artificial excess for the MOS compared to the pn because of the extra effective area and hence higher number of counts seen by the EPIC-pn detector. Therefore a limit of 250 source counts in the MOS cameras has been set to remove this bias.

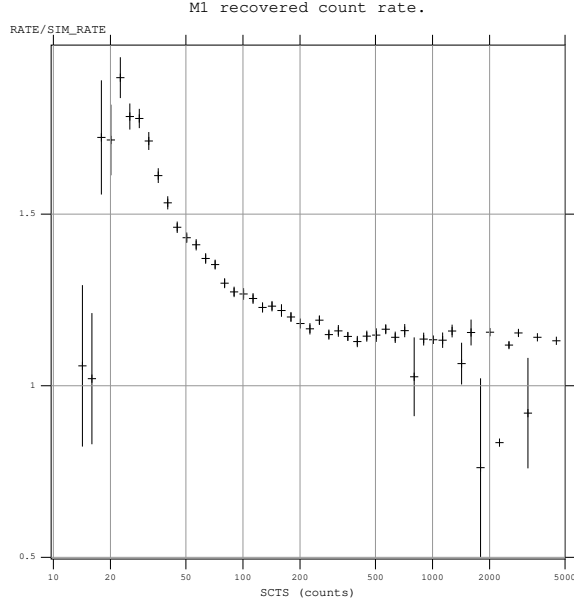


Figure 1: The ratio of detected to input counts from simulations involving the EPIC source parameterisation chain.

3 Method of flux determination

The flux (in units of $\text{ergs cm}^{-2} \text{s}^{-1}$) of a given source in a given energy band is given by

$$\text{Flux} = \text{counts} / \text{exposure_time} / \text{energy_conversion_factor} \quad (\text{i})$$

Counts are calculated by extracting the number of events from a circle around the source, subtracting the background and correcting for the fraction of the PSF outside the source circle (the encircled energy fraction or EEf).

$$\text{counts} = (\text{source_cnts_in_circle} - \text{background}) / \text{EEf} \quad (\text{ii})$$

The source is centroided and counts extracted from a circle of radius 18–28 arcseconds, dependent on source strength and off-axis angle.

Table 1: **Relative encircled energy factor for an on-axis source extracted from a circle of 20 arcsec radius.**

Camera	Energy	
	1.0 keV	7.0 keV
MOS-1	1.0	1.0
MOS-2	1.032	0.996
PN	1.046	1.057

3.1 Background subtraction

The background has been calculated for each catalogue field by removing all the detected sources and fitting a spline surface to the remaining image. This technique can introduce errors, especially when strong sources are present in the field.

3.2 The encircled energy fraction

The pipeline code uses a single model to represent the PSF of all three cameras. This is a reasonable approximation as the three telescopes are of very similar construction. In practise small differences will be present and are visible in parameterisations of the in-orbit PSF [3,4]. The relative EEf of the telescopes, predicted by these studies for an on-axis source, extracted with the mean radius used in the catalogue of 20 arcseconds is shown in Table 1. It is known that the King function, used in the PSF parameterisations, underpredicts the core of the real PSF and hence introduces an error in the EEf of small circles (or annuli). This effect, presumably different for each telescope, has not been quantified and so the values in Table 1 should only be used as a guideline.

3.3 The exposure time

This is calculated at the source centre from an exposure map which is derived from the sum of the frame times multiplied by the fractional exposure time, modulated by the spectrally dependent vignetting.

A correction for the dead-time due to the chip readouts which cause the out-of-time (OOT) event stripes has been applied to the exposure time by the source detection software.

3.4 Vignetting

Recent studies have shown that the optical-axis is not centred around a detector coordinate of DETX=0, DETY=0 as was previously supposed [5]. The best measurement of the

Table 2: The optical-axis positions used for recalculating the vignetting correction

Camera	DET-X	DET-Y
MOS-1	60	-230
MOS-2	400	-1350
PN	1250	280

Table 3: Percentage variation in PN v MOS flux ratio with spectral shape

Nh ^a	Index	Flux difference per band (%) ^b				
		1 (0.2-0.5 keV)	2 (0.5-2 keV)	3 (2.0-4.5 keV)	4 (4.5-7.5 keV)	5 (7.5-12.0 keV)
3	1.7	0.0	0.0	0.0	0.0	0.0
0	2.45	5.8	8.3	2.0	-2.6	-1.5
0	1.15	3.1	-2.3	-0.6	1.3	1.7
9.8	1.15	0.5	-5.0	-0.3	1.2	0.8
9.8	2.45	-3.3	2.4	1.5	-1.9	-1.4

^a Absorption column, 10^{20}cm^{-2} .

^b Fluxes calculated using the Thin filter matrices.

real optical-axis positions Table 2 have been used to recalculate the vignetting function and consequently the exposure time and source flux.

3.5 ECF

The energy conversion factors (ECF) have been reworked during this analysis (see SSC-LUX-TN-0059, issue 3.0 for the new values). They have been calculated assuming, what we expect to be, an average spectrum of an absorbed power law of slope $\Gamma = 1.7$ and $N_h = 3.0 \times 10^{20}\text{cm}^{-2}$. A deviation of source spectra from this average will affect the ECFs and modify the relative flux seen between the cameras. To quantify this effect we have performed a fit of an absorbed power-law on the band 2 (0.5–2 keV) spectra of 1900 PN sources detected over the field of view. The mean spectral slope is $\Gamma = 1.80 \pm 0.65$ (Fig. 2) and the limits on the absorption column which contain 1 sigma (68.3%) of the sources are $N_H = 0 - 9.8 \times 10^{20}\text{cm}^{-2}$ (Fig. 3). The effect of this dispersion in the source spectra on relative flux estimates is given in Table 3. It can be seen that the effect is small except in band 2, where an apparent excess of a few percent will be seen in the MOS cameras for a source spectrum flatter than the average and an excess in the PN camera will be seen if the spectrum is steeper, and band 1 where a smaller N_H will give an apparent increase in MOS flux. This can be understood from the shape of the effective area curves for MOS and PN (Fig. 4) which are reasonably parallel above 1.5 keV but diverge at lower energies.

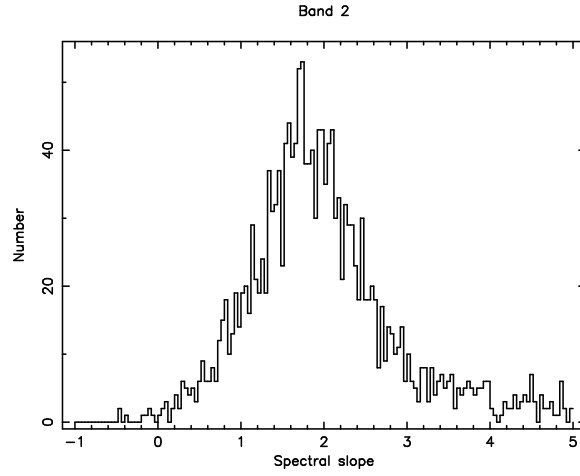


Figure 2: A histogram of spectral slopes derived from an absorbed power-law model fit to EPIC-pn spectra.

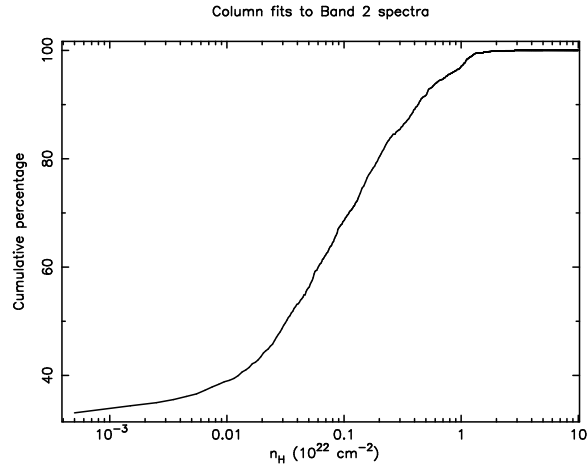


Figure 3: The distribution of n_H derived from an absorbed power-law model fit to EPIC-pn spectra.

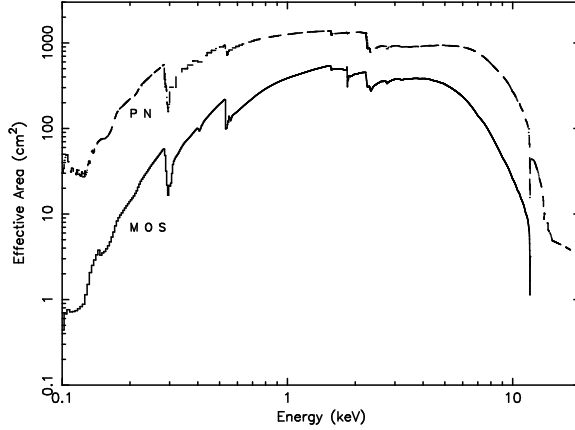


Figure 4: The effective area of the EPIC MOS and PN cameras with the Medium filter

These factors have been calculated using the on-axis redistribution matrices, *m11_im_all_2002-04-18.rmf*, *m21_im_all_2001-04-18.rmf* and *epn_ff20_sdY9.rmf* in conjunction with effective area files produced by `arfgen` using the quantum efficiency files, *EMOS1_QUANTUMEF_0014.CCF*, *EMOS2_QUANTUMEF_0014.CCF* and *EPN_QUANTUMEF_0012.CCF*. This form of calculating the ECFs makes the following implicit assumptions.

- The filter transmission is spatially invariant over the field
- The quantum efficiency of the detectors is spatially invariant
- Source counts are taken with event patterns 0-12 for the MOS and 0-4 for the PN (bands 2–5) and pattern 0 for PN band 1.

Pipeline images were actually created using event patterns 0–25 for MOS. The count rates extracted in the pipeline analysis therefore include patterns which are excluded in the ECF calculation. The effect of these extra events on the MOS ECFs is energy-dependent and is given as a set of percentages in Table 4. In this study, the extra patterns have been corrected for by increasing the ECFs and hence decreasing the EPIC fluxes by the factors in Table 4.

3.6 Outliers

Many sources exhibiting large flux differences between the cameras were evident in Version 1 of this study. From Figures 5 & 6 it can be seen that the situation is much improved in this version; this is principally due to the manual flagging present in the catalogue which allows suspect sources to be excluded from the sample. It should also be noted that

Table 4: The flux contribution of MOS pattern 13–25 events

Band	Correction percentage MOS
1	0.0
2	0.0
3	0.1
4	2.3
5	2.8

some problem fields, e.g. 0257/0112670601, which gave multiple sources with large flux differences in the previous study, were excluded from the construction of the catalogue. The major effect of the flagging has been to identify sources which lie close to CCD gaps, the edge of the field-of-view and bad pixels/columns.

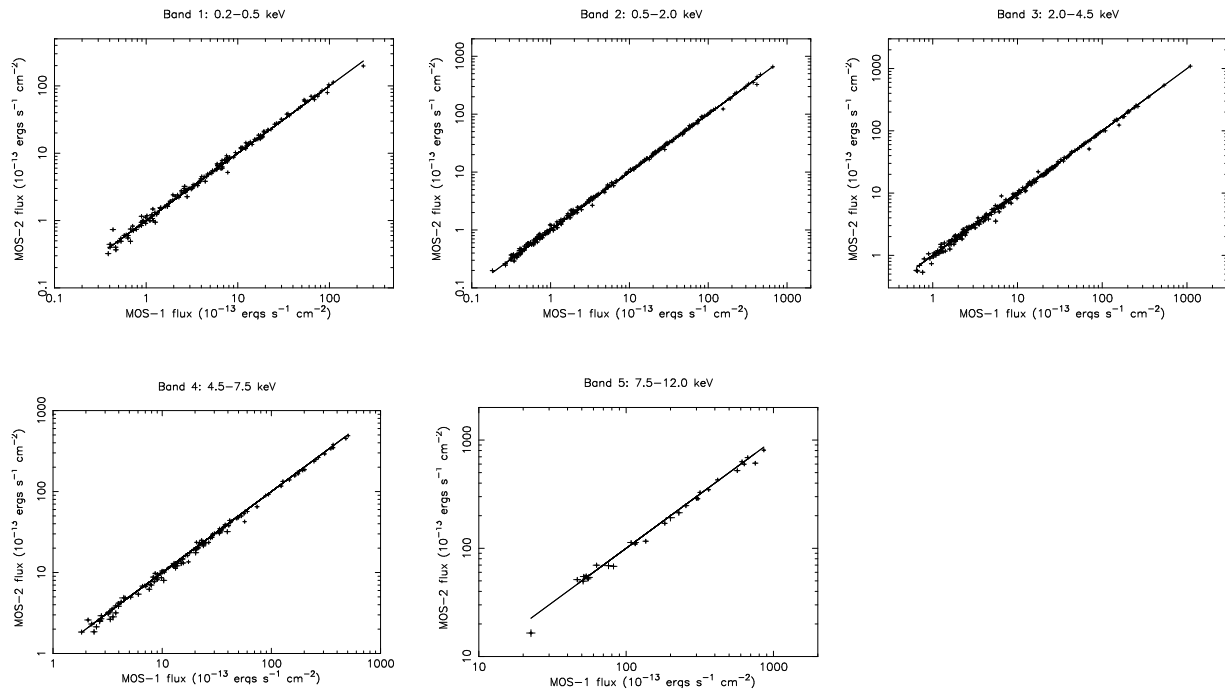


Figure 5: Observed flux in the EPIC MOS cameras

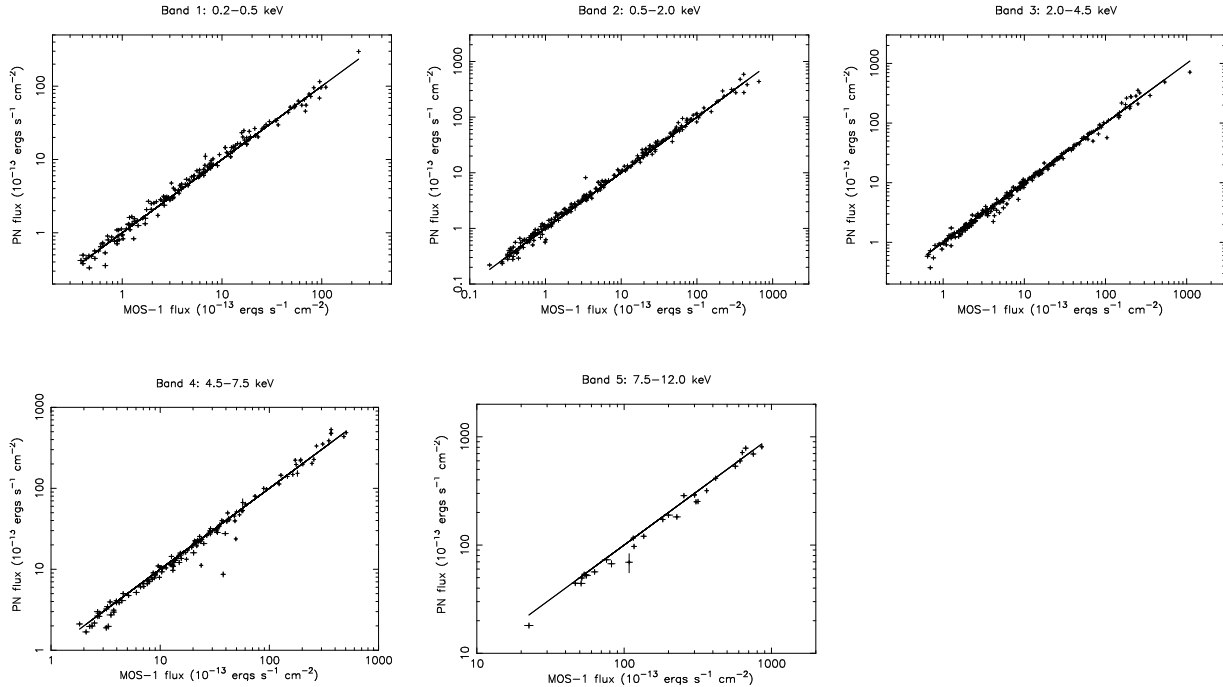


Figure 6: Observed flux in the EPIC PN and MOS-1 cameras

4 Results and Discussion

4.1 Mean offsets

A comparison of fluxes using the clean sample of sources described in section 2 is shown in Table 5. The MOS cameras are well calibrated with each other on-axis although MOS-1 records a small excess of flux at higher energies.

The MOS-PN on-axis comparison is good for the two low-energy bands. At energies above 2 keV the two MOS cameras predict 5–10% more flux than EPIC-pn. This was seen in the previous study where the MOS excess was ascribed to errors in the quantum efficiency (QE) of one or all the cameras. The QE has been reexamined and modified for each camera [6,7] recently but clearly has not resolved the discrepancy. The vignetting function has also received considerable attention since the last study and the optical-axis shifts, applied here, should remove this as a source of possible error. Catalogue fluxes have been produced using the encircled energy fraction calculated from the MEDIUM mode PSF, which is identical for each camera. The effects of this simplification were discussed in section 3.2 and estimated in Table 1. If taken at face value these discrepancies introduce an offset of $\sim 3-6\%$ in the EPIC-pn fluxes which will significantly improve the comparison

Table 5: **The mean on-axis flux differences in the EPIC cameras.**

Band	Energy (keV)	Mean flux difference (%) ^a		
		(M1-M2)/M1	(M1-PN)/PN	(M2-PN)/PN
1	0.2–0.5	-1.4 ± 0.5	2.6 ± 0.7	4.4 ± 0.7
2	0.5–2.0	-1.6 ± 0.4	0.6 ± 0.7	3.0 ± 0.7
3	2.0–4.5	1.8 ± 0.4	8.8 ± 0.6	7.6 ± 0.6
4	4.5–7.5	3.2 ± 0.6	7.9 ± 0.8	5.3 ± 0.8
5	7.5–12.0	3.0 ± 1.2	10.9 ± 1.5	8.9 ± 1.5

^a The percentage flux difference between the cameras using the source sample described in section 2. Errors quoted are 90% for 1 free parameter.

Table 6: **The mean flux differences for band 2 for different source populations.**

cnts in MOS	offax (arcmin)	Mean flux difference (%)		
		(M1-M2)/M1	(M1-PN)/PN	(M2-PN)/PN
50–250	0–5	1.0 ± 0.9	4.9 ± 0.6	7.1 ± 0.7
50–250	5–12	4.3 ± 0.5	7.5 ± 0.4	7.2 ± 0.4
250–10000	0–5	-1.6 ± 0.4	0.6 ± 0.7	3.0 ± 0.7
250–10000	5–12	2.7 ± 0.5	6.1 ± 0.5	4.8 ± 0.6

with the MOS. Application of these values would, however, give a $\sim 4\%$ excess of MOS-2 over MOS-1 in bands 1 and 2.

The effects of using fainter sources for the flux comparison has been investigated for band 2 (Table 6). This shows a widening of the discrepancy between the MOS and PN cameras in agreement with the effect of low-counts on measured fluxes discussed in section 2.1.

A sample of sources at off-axis angles of 5–12 arcminutes (i.e. excluding the central chip of the MOS cameras) has been analysed. The band 2, MOS/PN difference for this sample is $\sim 6\%$.

4.2 Dispersion

In this study we have access to a sufficient number of sources to investigate the dispersion of the flux differences. This number reflects the total systematic error involved with the measurement of each camera flux which in turn allows a comparison to be made between the estimated systematics for each calibration quantity [8] and the actual performance of the system.

It can be seen immediately from Figs. 7 & 8 that the MOS-PN distribution is significantly broader than that of the two MOS cameras. As shown in section 3.5 the distributions of bands 1 and 2 are influenced by spectral shape and so we have selected band 3 fluxes, to investigate instrumental uncertainties. The total percentage error may be obtained from

Table 7: **The dispersion of the band-3 flux difference distribution**

Selection		M1/M2		M1/PN		M2/PN	
cnts	offax ^a	sigma ^b	syserr ^c	sigma	syserr	sigma	syserr
250–10000	0–5	1.32 ± 0.08	2.7 ± 0.2	1.94 ± 0.20	4.9 ± 0.2	1.79 ± 0.16	5.0 ± 0.2
250–10000	5–12	1.51 ± 0.17	7.3 ± 0.5	0.88 ± 0.16	0.0 ± 1.9	1.28 ± 0.17	5.2 ± 0.9
50–250	0–5	1.29 ± 0.06	10.3 ± 0.7	1.15 ± 0.05	7.2 ± 0.8	1.33 ± 0.07	11.4 ± 0.7
50–250	5–12	1.37 ± 0.06	13.7 ± 0.6	1.23 ± 0.06	9.5 ± 0.8	1.28 ± 0.06	10.7 ± 0.7

^a Off-axis angle range (arcminutes).

^b The width of the flux difference distribution in units of the statistical error.

^c The systematic error calculated from the width of the flux difference distribution (%).

Table 8: **Estimated systematic errors in calibration quantities**

Effect	MOS-1		MOS-2		PN	
	On-axis	Off-axis	On-axis	Off-axis	On-axis	Off-axis
PSF ^a	1	4	1	4	1	2
Vignetting ^b	1	1.5	1	1.5	1	1.5
Spectrum [band 2]	0	0	0	0	7	7
Spectrum [band 3]	0	0	0	0	1.5	1.5

^a The spread in flux due to the uncertainties introduced by the MEDIUM mode PSF encircled energy correction used in the pipeline. The values for the MOS off-axis reflect the individual placement of each CCD which results in an azimuthal variation not reflected in the calibration.

^b The spread in flux caused by the residual uncertainty of 10 arcseconds in the position of the optical axes.

Figures 7 & 8 and the systematic error of the combined measurement derived by subtracting the statistical error of each flux pair (Table 7). The dispersion of the MOS-1/MOS-2 stronger near-on-axis sources is $\sim 2\%$ and is consistent with residual uncertainties in the vignetting and PSF functions (see Table 8). A larger systematic error is evident for fainter sources which is associated with the effect of low-counts as discussed in section 2.1 and also by errors introduced in the processing, such as the background subtraction (see section 3.1) which will gain in importance at low fluxes. The off-axis systematic error rises to $\sim 6\%$ for the stronger detections; which can be explained by an uncertainty introduced in the off-axis PSF of the MOS cameras. As noted in section 3.2 the same PSF is used for all three cameras and is only dependent on off-axis angle and photon energy. The MOS CCDs have been placed in three layers to follow the focal surface which means that the PSF of the outer CCDs is azimuthally dependent [9]. This introduces a $\sim \pm 4\%$ error in the encircled energy fraction contained in a 20 arcsecond circle.

The derived MOS/PN systematic errors are larger ($\sim 5\%$) with apparently little dependence on off-axis angle. Off-axis this is consistent with the expected instrumental systematics, again principally due to the off-axis PSF of the MOS cameras. It is not clear why the on-axis dispersion should be so broad; this result implies an unknown random element of magnitude 3–4% in the MOS/PN flux ratio.

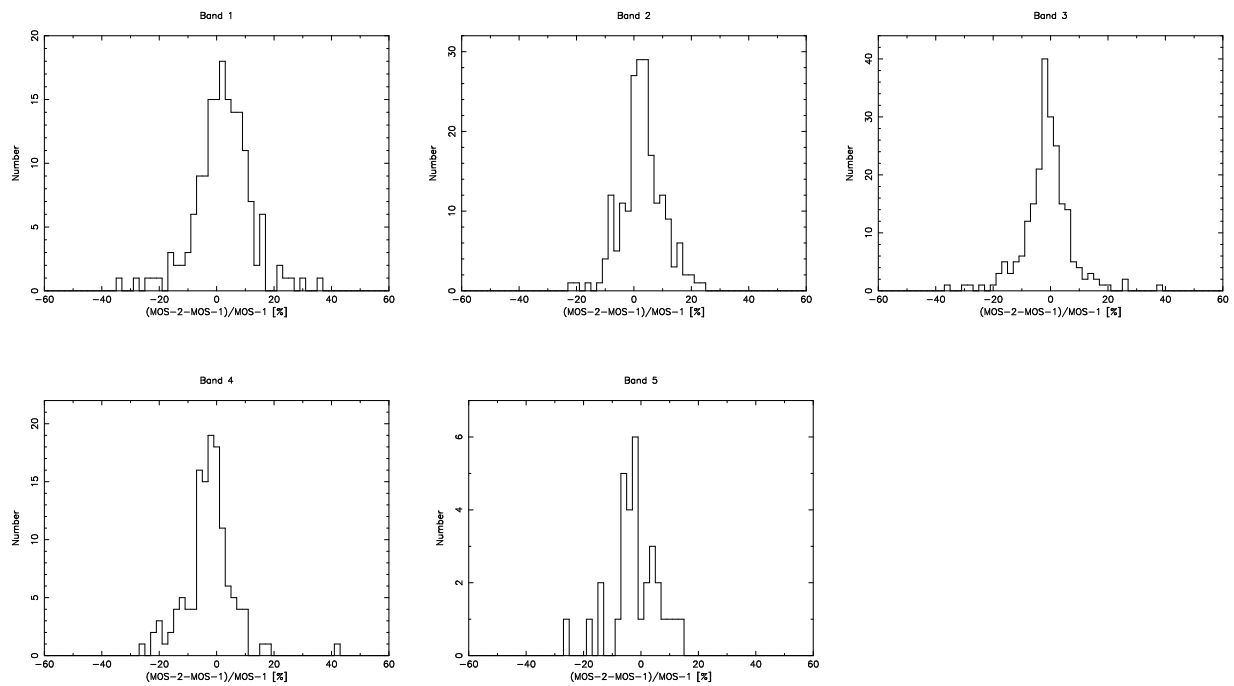


Figure 7: Percentage flux difference in the EPIC MOS cameras $[(\text{Mos-2} - \text{Mos-1}) / \text{Mos-1}]$

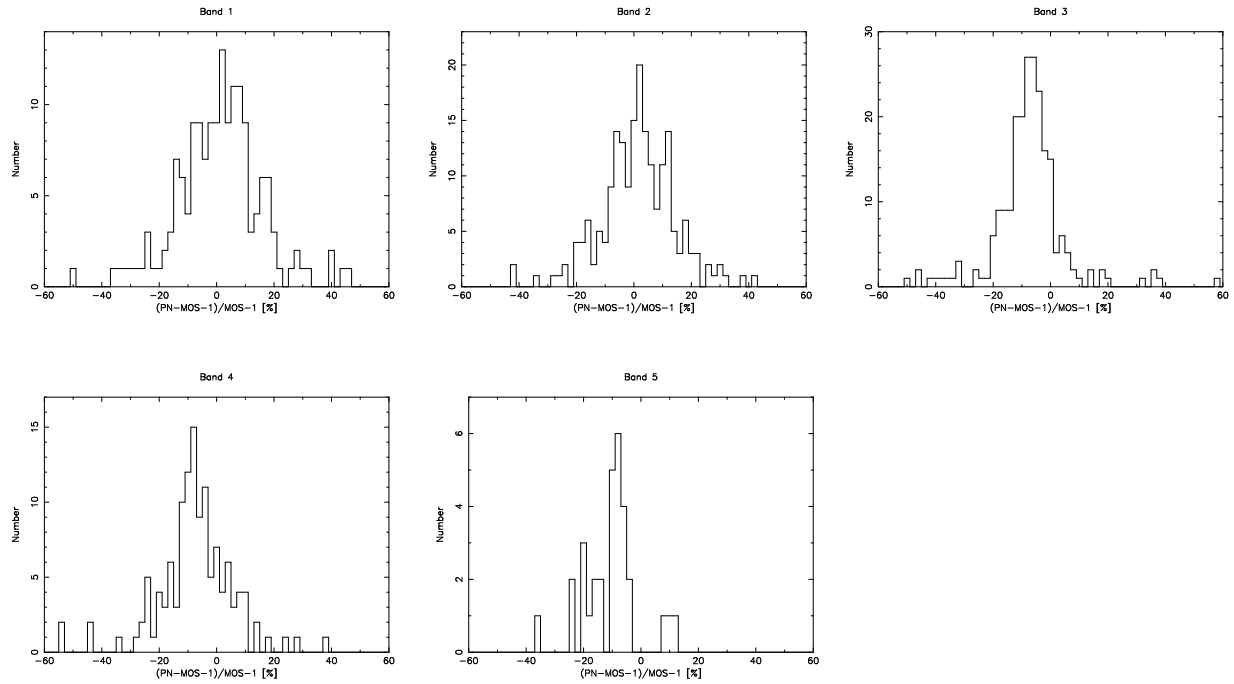


Figure 8: Percentage flux difference in the EPIC MOS-1 and PN cameras $[(\text{PN} - \text{Mos-1}) / \text{Mos-1}]$

5 Conclusions

The MOS cameras appear to be well calibrated with respect to each other except for a small excess in MOS-1 at high energies. The dispersion of the flux ratio distribution is small and consistent with expected instrumental systematics on axis. Off-axis the dispersion is broader but can be reasonably interpreted as errors introduced by an azimuthal variation in the MOS PSF which is not currently modelled.

Both MOS cameras show a significant excess of flux compared with EPIC-pn above 2 keV. This may be partly due to the simplified PSF used in the calculation of catalogue fluxes and partly due to an unknown element, possibly the MOS QE or the grating obscuration factor. Off-axis, the flux difference between the cameras is greater. The dispersion of the MOS/PN distribution is broader than that of the two MOS cameras; off-axis it is compatible with the expected instrumental uncertainties but there appears to be an unknown element of 3 – 4% which is affecting the on-axis dispersion.

5.1 Pipeline, catalogue and calibration issues

This study has exposed the following issues with the calculation of source fluxes by the pipeline.

- The current erroneous positioning of the optical-axes strongly affects measured source flux, particularly off-axis and should be corrected.
- The PSF measured from in-orbit data should be used to calculate the encircled energy fraction.
- A greater effort needs to be spent on quantifying the off-axis EPIC PSF, particularly the azimuthal, chip-to-chip, variations present in the MOS detector.
- Fluxes calculated from low numbers of source counts are biased due to selection effects.

Acknowledgements. This survey has been made possible by the quality and consistency of the pipeline and source searching software developed by Hermann Brunner, Jean Ballet, Michael Freyberg, Matthias Ehle, Dean Hinshaw, Georg Lamer and Uwe Lammers. Thanks are also due to all the members of the SSC who have helped to produce the 1XMM catalogue in record time. Finally, I'd like to express my appreciation for the rigorous simulation work undertaken by Ian Stewart which has illuminated and quantified the subtle effects of low source counts on measure flux.

References

- [1] Watson, M.G., et al. 2003, *Astron. Nachr.*, 324, 89

- [2] Watson, M.G., et al. 2001, "The XMM-Newton Serendipitous survey: 1. The role of XMM-Newton Survey Science Centre", A&A, 365, L51.
- [3] Ghizzardi, S., "In-flight calibration of the on-axis and near off-axis PSF for the Mos-1 and Mos-2 cameras", EPIC-MCT-TN-011.
- [4] Ghizzardi, S., "In-flight calibration of the PSF for the PN camera", EPIC-MCT-TN-012.
- [5] D. H. Lumb, A. Finoguenov, R. Saxton, B. Aschenbach, P. Gondoin, M. Kirsch, I. M. Stewart, 2003, "In-orbit Calibrations of XMM-Newton Telescopes", Proc SPIE 4851 2003 in press
- [6] Saxton, R., Lumb, D., "EPIC spectral Response Distribution", XMM-SOC-CAL-SRN-0121.
- [7] Saxton, R., "EPIC pn quantum efficiency", XMM-SOC-CAL-SRN-0139.
- [8] Kirsch, M., "EPIC status of calibration and data analysis", XMM-SOC-CAL-TN-0018.
- [9] Saxton, R.D., Denby, M., Griffiths, R.G., Neumann, D.M., 2003, Astron. Nachr., 324, 138.